Final report

DOE Award number: DE-SC0019255

Recipient Name: Regents of the University of Michigan
Project Title: LaserNetUS
PD/PI Name : Professor Karl Krushelnick

Contact information:
Center for Ultrafast Optical Science, University of Michigan
2200 Bonisteel Boulevard, Ann Arbor
Michigan 48109
Email: kmkr@umich.edu
Phone: (734) 763-4877
Fax: (734) 763-4876

Project Period: August 18. 2018 - August 17, 2020

Report Submission Date: November 15, 2019

Reporting period (Start and End Date): Aug. 18 2018 – Aug. 17 2020

Abstract.

In this proposal we have formed a consortium in response to a request from the DoE Office of Fusion Energy Sciences to establish a national network of Petawatt-class laser systems to act as domestic user facilities that can enable a broad range of frontier scientific research. This new entity is called LaserNet US. The network formed here is directly responsive to recommendations made in a recently released National Academy of Sciences Report with regard to US strategy for high intensity laser research, "Opportunities in Intense Ultrafast Lasers: Reaching for the Brightest Light". As detailed in this report, the research in this area has the potential to transform science in a number of research fields and to open up new areas of fundamental research. High field science was initiated in the US in the 1990's, and subsequently Europe and Asia have embraced this research field, investing more than a billion dollars in this area over the past several years.

Our network includes five academic and two national lab-based high intensity laser facilities. These facilities are distributed geographically throughout the US and the network provides access to complementary facilities which have unique world-class laser and experimental capabilities. LaserNet US will make these existing Petawatt-class laser facilities available to users from around the country who until now have not had regular access to such machines. Consequently, the network, which will develop over time, will also become a key element in driving forward national research in high field and high energy density plasma science.

In particular, the University of Michigan provides access to the Hercules laser facility and the T-cubed laser facility for collaborative experiments as part of the first year operation. In the second year – to begin in summer 2019 – the experiments will be chosen via proposal submission and review by an outside panel formed by DOE.

Results

The LaserNetUS Network was established and the first experiments were performed on the laser facilities at Michigan (as well as at the other facilities). These experiments were successful and publications are in preparation as a result of this work. The network had a Kickoff meeting in Lincoln Nebraska in August 2018 – and has had bi-weekly conference calls since that time for managing the operation of the network.

A proposal review panel was also set up and two proposal calls were initiated. Six experiments were chosen for the Hercules facility at the University of Michigan. Two experiments were successfully completed and results from those experiments are described below. These results and related research have been published in the papers:

1) K. Krushelnick, A. G. R. Thomas, L. Williingale, "LaserNet re-invigorates high intensity laser research", *Photonics Spectra*, June pg. 68 (2019).
2) Ma, Y., Seipt, D., Hussein, A. E., Hakimi, S., Beier, N. F., Hansen, S. B., Hinojosa, J., Maksimchuk, A., Nees, J., Krushelnick, K., Thomas, A. G. R., Dollar, F. "Polarization-Dependent Self-Injection by Above Threshold Ionization Heating in a Laser Wakefield Accelerator", Physical Review Letters 124 114801 (2020).
3) Vais, O. E., Thomas, A. G. R., Maksimchuk, A. M., Krushelnick, K., Bychenkov, V. Yu "Characterizing extreme laser intensities by ponderomotive acceleration of protons from rarified gas" New Journal of Physics 22, 023003 (2020).

4) M. J.-E. Manuel, H. Tang, B. K. Russell, L. Willingale, A. Maksimchuk, J. S. Green, E. L. Alfonso, J. Jaquez, L. Carlson, D. Neely, and T. Ma , "Enhanced spatial resolution of Eljen-204 plastic scintillators for use in rep-rated proton diagnostics" (accepted for publication in *Review of Scientific instruments* 2020)
5) Ma, Y., Seipt, D., Hussein, A. E., Hakimi, S., Beier, N. F., Hansen, S. B., Hinojosa, J., Maksimchuk, A., Nees, J., Krushelnick, K., Thomas, A. G. R., Dollar, F. "Role of polarization-dependent ionization on injection dynamics of a laser wakefield accelerator", submitted to special edition of Physics of Plasmas, 2020 (also invited talk at APS/Division of Plasma Physics annual meeting November, 2020).

Because of an ongoing upgrade of the Hercules Laser system until the end of 2019 the start of the other four experiments were delayed. In addition, because of the coronavirus pandemic no visitors have been allowed onto the University of Michigan campus since March 2020. Consequently the third experiment only started in October 2020 and the other three will not be completed until May 2021.

Experiment 1-2019, LaserNetUS: HERCULES Experiment

Warm Wave Breaking Injection in Laser Wakefield Acceleration

PI : Professor Franklin Dollar: Dept. of Physics, University of California, Irvine
Nicholas F. Beier, Sahel Hakimi (graduate students – UC Irvine)

Other contributors:
Y. Ma, D. Seipt, A. E. Hussein (grad student), J. Hinojosa (grad student), A. Maksimchuk, J. Nees, K. Krushelnick, A. G. R. Thomas
Center for Ultrafast Optical Science, University of Michigan, Ann Arbor, Michigan 48109, USA

We report the first experimental observation of a lowering of the self-injection threshold with a warm plasma generated by a circular polarized (CP) laser pulse in laser-wakefield acceleration. We have found that a self injected electron beam can be observed with a CP laser pulse at a plasma density lower than the self-injection threshold for a linearly polarized (LP) laser pulse. By varying the plasma density, the self-injection density threshold for CP laser is much lower than that of the LP laser pulse in both low and high power cases. When the laser power and plasma density is high enough for self-injection, the total beam charge with a CP laser can be an order of magnitude higher than that with a LP laser. Particle-in-Cell (PIC) simulations have confirmed the theoretical prediction that thermal effects of warm plasma with temperature on the orders of 10-100 eV can lead to significant enhancement of the trapping and injection efficiency.

Laser-wakefield acceleration (LWFA) [1] has experienced a rapid development over the last decade owing to its ability to produce multi-GeV electron beams [2-4]. Such high energy electron beams also have the capability to drive secondary particle and radiation sources, such as positrons [5], betatron X-rays [6], and collimated gamma-rays from inverse Compton scattering [7, 8] and even opening the door to experimental studies of nonlinear QED [9, 10]. It can also be a promising alternative for seeding compact X-ray free electron lasers (XFEL). However, such applications place significant requirements on the beam quality in terms of energy spread, emittance, beam charge and shot-to-shot stability, especially for seeding XFELs [11, 12].

The control of the electron beam quality mostly relies on the injection process and the

subsequent beam dynamics within the plasma. In LWFA, especially in the nonlinear “bubble" regime [13, 14], the electrons in the background which are expelled transversely by the laser ponderomotive force slip back to the rear of the bubble and are trapped by the wake field since their longitudinal velocity is higher than the phase velocity of the plasma wave. This is the so-called “self-injection" mode of operation.

Theoretical and numerical simulation studies indicate that there exist thresholds on laser intensity and plasma density for self-injection. Due to the laser pulse evolution - hence the plasma wave evolution - it is normally difficult to control the self-injection process. Therefore, to lower the threshold of self-injection and to better control the injection process, various injection schemes such as pondermotive injection [15], colliding pulse injection [16,18], ionization injection [19], density transition injection [20] and two-color injection [21] have been proposed.

However, self-injection is still the simplest scheme from an experimental point of view. Therefore the dynamics of self-injection have been studied extensively. Theoretical and numerical simulation studies has shown that the trapping threshold can be lowered with warm plasma [22, 23]. Warm plasma can be produced with either a heater [24] to pre-ionize the gas medium or by using a circular polarized laser pulse in which case the laser pulse is both the driver for the wakefield and the heater for the warm plasma. Normally the influence of the laser polarization on the formation of wakefield is negligible since the driving ponderomotive force is isotropic in the transverse direction to laser propagation. However, the net transverse momentum gain of electrons passing through the laser field is much lower for LP laser than for CP laser.

In this present work, we investigate the role of the plasma temperature (resulting from the laser polarization during ionization) in electron trapping in LWFA by comparing the total beam charge with linear-polarized (LP) and circular-polarized (CP) laser pulses. Plasma emission spectroscopy indicates a higher plasma temperature with circular-polarized laser pulse than that with linear-polarized laser pulse. We also found that the self-injected electron beams can be observed with a CP laser pulse at a plasma density much lower than the self-injection threshold for a LP laser pulse.

By varying the plasma density, the self-injection density threshold for a CP laser is much lower than that of LP laser for both low and high power cases. When the laser power and plasma density is high enough for self-injection, the total beam charge with CP laser can be an order of magnitude higher than that with LP laser. Particle-in-Cell (PIC) simulations confirmed the theoretical predication that the thermal effect of warm plasma with temperature on the orders of 10 - 100 eV could lead to significant enhancement of the trapping and injection efficiency [25].

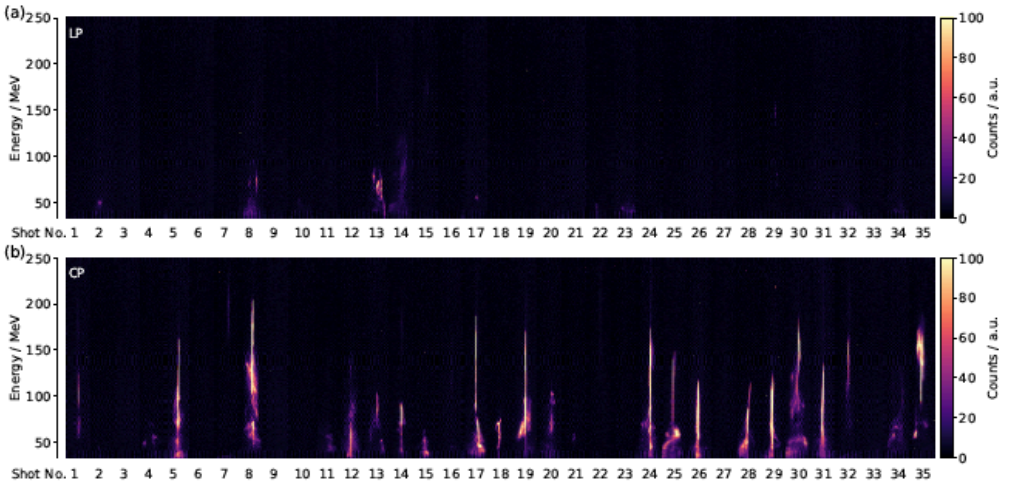

FIG. 1. *Electron spectra of 35 consecutive shots with (a) linear polarized and (b) circular polarized laser beam taken at roughly the same laser power P = 50 TW and plasma density* n_e = $3.8 \times 10^{18} cm^{-3}$.

The experiment was performed at the HERCULES laser facility at the Center for Ultrafast Optical Science (CUOS) at the University of Michigan [26]. The laser beam with an averaged power of P_L = 80 TW after compression was focused by an f/20 off-axis paraboloid (OAP) to a spot size of w_0 = 24 μm ($1/e^2$ in intensity).

The laser pulse duration is about 34 fs (FWHM) at best compression. The corresponding peak laser intensity is about 5.6×10^{18} W/cm^2 which gives a normalized laser intensity a_0 = 1.6 for LP laser. The target was a 3D-printed length-variable gas-cell [27] filled with pure helium. The use of the gas-cell and low-Z gas is to suppress self-injection caused by plasma density ripples, which often happens with supersonic gas jet targets [28], and ionization injection. The plasma density was characterized with a Mach-Zehnder interferometer with a probe beam arriving at the target 20 ps after the main beam. The plasma density can be expressed as $n_p[10^{18} cm^{-3}]$ = 0.05 x P [psi], where P is the backing pressure. To switch the laser polarization between LP and CP, a 1 mm thick 1/4 wave plate was placed into the beam path before the OAP. By rotating the axis of the plate by 45 degrees the polarization direction can be easily switched without causing any difference in the laser intensity and focal spot quality. The electron energy spectra were measured by using an electron spectrometer which is composed of a dipole magnet (15 cm long, 0.8 T), a piece of Lanex screen and a 12-bit CCD camera. The dispersion of the electron spectrometer (electron energy as a function of position on Lanex screen) was determined by a particle trajectory tracking code with the measured magnetic field of the magnet. To determine the electron beam charge, the Lanex signal was calibrated by using Fuji BAS-MS image plate [29] which gives 2:9 x 10^{-6} pC/count [30]. A flat-field spectrometer [31] composed of a gold-coated diffraction grating and a 16-bit CCD was placed 3 m away from the target to collect the on-axis plasma emission in a spectral range of 5 - 30 nm. The intensity ratio of the characteristic emission lines can be used to retrieve the plasma temperature [32].

Comparison of the electron spectra with a CP and an LP laser at the same laser intensity and plasma density is illustrated in Fig. 1. For a laser power of P = 50 TW and a plasma density of $n_p = 3.8 \times 10^{18} cm^{-3}$, the ratio of the laser power to the critical power for self-guiding is P/P_c = 7.7, where P_c [GW] = 17.4 (n_c/n_p) [33], n_c is the critical density for the laser frequency. This ratio is lower than the injection threshold of P/P_c = 8.5 for the LP laser in our case, so self- injection with LP laser would be avoided. As shown in Fig. 1(a), the reproductibility

with the LP laser pulse is only about 10% with very poor beam quality and an averaged beam charge of 1.59 pC. Here the relative large error comes from the fact that electron beam is absent in most of the shots in this situation. While with CP laser, as in Fig. 1(b), the reproducibility of an electron beam with energies higher than 50 MeV increased to about 70% with an averaged beam charge of 8.6 pC.

Fig. 2 shows the electron beam charge as a function of plasma density with the same laser power as in Fig. 1. The self-injection threshold density lowered from 5.2 x 10^{18}cm^{-3} for LP laser to 3.2 x 10^{18}cm^{-3} for CP laser. Consequently, the threshold ratio of laser power to critical power for self-guiding P/P_c is lowered from 8.5 for a LP laser to 5.1 for CP laser, which is comparable with the reported value in Ref.[34]. The simulations were performed with the quasi-3D FBPIC code [35] which is "numerical dispersion free" in all directions to avoid injection caused by numerical noise.

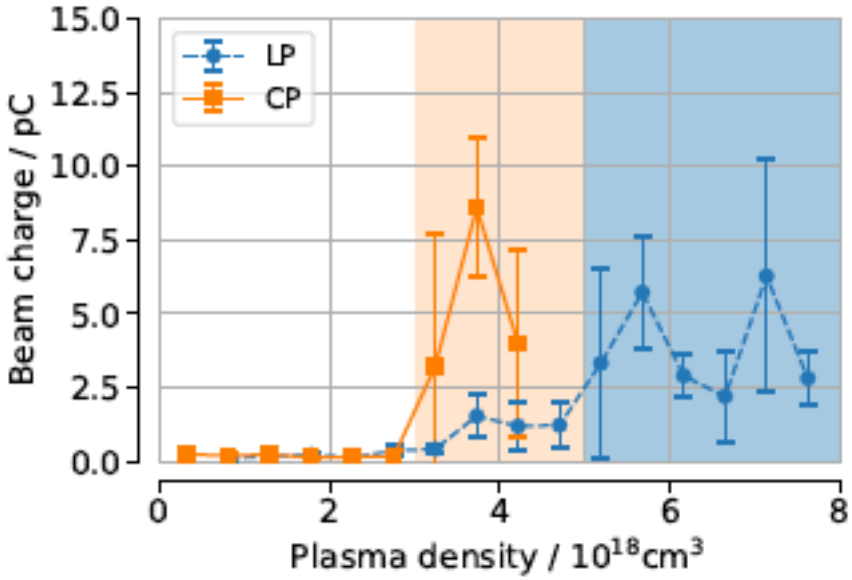

FIG. 2. *Electron beam charge as a function of plasma density with LP laser (blue circles) and CP laser (orange squares) with the same laser power of P = 50 TW. Note that the large error bars come from the fact that there are still shots with no electron beam observed even above the injection threshold in both cases.*

[1] T. Tajima and J. M. Dawson, *Phys. Rev. Lett*. **43**, 267 (1979).
[2] W. P. Leemans, A. J. Gonsalves, H.-S. Mao, K. Nakamura, C. Benedetti, C. B. Schroeder, C. Toth, J. Daniels, D. E. Mittelberger, S. S. Bulanov, J.-L. Vay, C. G. R. Geddes, and E. Esarey, *Phys. Rev. Lett.* **113**, 245002 (2014).
[3] H. T. Kim, K. H. Pae, H. J. Cha, I. J. Kim, T. J. Yu, J. H. Sung, S. K. Lee, T. M. Jeong, and J. Lee, *Phys. Rev. Lett*. **111**, 165002 (2013).
[4] X. Wang, R. Zgadzaj, N. Fazel, Z. Li, S. A. Yi, X. Zhang, W. Henderson, Y. Y. Chang, R. Korzekwa, H. E. Tsai, C. H. Pai, H. Quevedo, G. Dyer, E. Gaul, M. Martinez, A. C. Bernstein, T. Borger, M. Spinks, M. Donovan, V. Khudik, G. Shvets, T. Ditmire, and M. C. Downer, *Nature Communications* **4**, 1988 (2013).
[5] G. Sarri, W. Schumaker, A. Di Piazza, M. Vargas, B. Dromey, M. E. Dieckmann, V. Chvykov, A. Maksimchuk, V. Yanovsky, Z. H. He, B. X. Hou, J. A. Nees, A. G. R. Thomas, C. H. Keitel, M. Zepf, and K. Krushelnick, *Phys. Rev. Lett.* **110**, 255002 (2013).
[6] S. Kneip, C. McGuffey, J. L. Martins, S. F. Martins, C. Bellei, V. Chvykov, F. Dollar, R. Fonseca, C. Huntington, G. Kalintchenko, A. Maksimchuk, S. P. D. Mangles, T. Matsuoka, S. R.

Nagel, C. A. J. Palmer, J. Schreiber, K. T. Phuoc, A. G. R. Thomas, V. Yanovsky, L. O. Silva,K. Krushelnick, and Z. Najmudin, *Nature Physics* **6**, 980 (2010).
[7] W. Yan, C. Fruhling, G. Golovin, D. Haden, J. Luo, P. Zhang, B. Zhao, J. Zhang, C. Liu, M. Chen, S. Chen, S. Banerjee, and D. Umstadter, *Nat. Photonics* **11**, 514 (2017).
[8] G. Sarri, D. J. Corvan, W. Schumaker, J. M. Cole, A. Di Piazza, H. Ahmed, C. Harvey, C. H. Keitel, K. Krushelnick, S. P. D. Mangles, Z. Najmudin, D. Symes, A. G. R. Thomas, M. Yeung, Z. Zhao, and M. Zepf, *Phys. Rev. Lett.* **113**, 224801 (2014).
[9] J. M. Cole, K. T. Behm, E. Gerstmayr, T. G. Blackburn, J. C. Wood, C. D. Baird, M. J. Du_, C. Harvey, A. Ilderton, A. S. Joglekar, K. Krushelnick, S. Kuschel, M. Marklund, P. McKenna, C. D. Murphy, K. Poder, C. P. Ridgers, G. M. Samarin, G. Sarri, D. R. Symes, A. G. R. Thomas, J. Warwick, M. Zepf, Z. Najmudin, and S. P. D. Mangles, *Phys. Rev. X* **8**, 011020 (2018).
[10] K. Poder, M. Tamburini, G. Sarri, A. Di Piazza, S. Kuschel, C. D. Baird, K. Behm, S. Bohlen, J. M. Cole, D. J. Corvan, M. Duff, E. Gerstmayr, C. H. Keitel, K. Krushelnick, S. P. D. Mangles, P. McKenna, C. D. Murphy, Z. Najmudin, C. P. Ridgers, G. M. Samarin, D. R. Symes, A. G. R. Thomas, J.Warwick, and M. Zepf, *Phys. Rev. X* **8**, 031004 (2018).
[11] F. Gruner, S. Becker, U. Schramm, T. Eichner, M. Fuchs, R.Weingartner, D. Habs, J. Meyer-ter Vehn, M. Geissler, M. Ferrario, L. Serafini, B. van der Geer, H. Backe, W. Lauth, and S. Reiche, *Applied Physics B* **86**, 431 (2007).
[12] A. Bernhard, V. A. Rodrguez, S. Kuschel, M. Leier, P. Peiffer, A. Svert, M. Schwab, W. Werner, C. Widmann, A. Will, A.-S. Mller, and M. Kaluza, *Nuclear Instruments and Methods in Physics Research Section A: Accelerators, Spectrometers, Detectors and Associated Equipment* **909**, 391 (2018), 3rd European Advanced Accelerator Concepts workshop (EAAC2017).
[13] A. Pukhov and J. Meyer-ter Vehn, *Applied Physics B* **74**, 355 (2002).
[14] W. Lu, M. Tzoufras, C. Joshi, F. S. Tsung, W. B. Mori, J. Vieira, R. A. Fonseca, and L. O. Silva, *Phys. Rev. ST Accel. Beams* **10**, 061301 (2007).
[15] D. Umstadter, J. K. Kim, and E. Dodd, *Phys. Rev. Lett*. **76**, 2073 (1996).
[16] E. Esarey, R. F. Hubbard, W. P. Leemans, A. Ting, and P. Sprangle, *Phys. Rev. Lett*. **79**, 2682 (1997).
[17] G. Fubiani, E. Esarey, C. B. Schroeder, and W. P. Leemans, *Phys. Rev. E* **70**, 016402 (2004).
[18] H. Kotaki, S. Masuda, M. Kando, J. K. Koga, and K. Nakajima, *Physics of Plasmas* **11**, 3296 (2004), https://doi.org/10.1063/1.1751171.
[19] M. Chen, Z. M. Sheng, Y. Y. Ma, and J. Zhang, *Journal of Applied Physics* **99**, 1 (2006).
[20] S. Bulanov, N. Naumova, F. Pegoraro, and J. Sakai, *Phys. Rev. E* **58**, R5257 (1998).
[21] L.-L. Yu, E. Esarey, C. B. Schroeder, J.-L. Vay, C. Benedetti, C. G. R. Geddes, M. Chen, and W. P. Leemans, Phys. Rev. Lett. 112, 125001 (2014).
[22] E. Esarey, C. B. Schroeder, E. Cormier-Michel, B. A. Shadwick, C. G. Geddes, and W. P. Leemans, Physics of Plasmas 14 (2007), 10.1063/1.2714022.
[23] C. Benedetti, C. B. Schroeder, E. Esarey, F. Rossi, and W. P. Leemans, *Physics of Plasmas* **20**, 103108 (2013), https://doi.org/10.1063/1.4824811.
[24] J. Daniels, A. J. Gonsalves, C. V. Pieronek, C. Benedetti, J. van Tilborg, C. B. Schroeder, and W. P. Leemans, *AIP Conference Proceedings* **1812**, 040008 (2017), https://aip.scitation.org/doi/pdf/10.1063/1.4975855.
[25] E. Esarey, C. B. Schroeder, E. Cormier-Michel, B. A. Shadwick, C. G. R. Geddes, and W. P. Leemans, *Physics of Plasmas* **14**, 056707 (2007), https://doi.org/10.1063/1.2714022.
[26] T. Z. Zhao, K. Behm, C. F. Dong, X. Davoine, S. Y. Kalmykov, V. Petrov, V. Chvykov, P. Cummings, B. Hou, A. Maksimchuk, J. A. Nees, V. Yanovsky, A. G. R. Thomas, and K. Krushelnick, *Phys. Rev. Lett.* **117**, 094801 (2016).
[27] M. Vargas, W. Schumaker, Z.-H. He, Z. Zhao, K. Behm, V. Chvykov, B. Hou, K. Krushelnick, A. Maksimchuk, V. Yanovsky, and A. G. R. Thomas, *Applied Physics Letters* **104**,

174103 (2014), https://doi.org/10.1063/1.4874981.
[28] S. Kuschel, M. B. Schwab, M. Yeung, D. Hollatz, A. Seidel, W. Ziegler, A. S□avert, M. C. Kaluza, and M. Zepf, *Phys. Rev. Lett.* **121**, 154801 (2018).
[29] N. Nakanii, K. Kondo, T. Yabuuchi, K. Tsuji, K. A. Tanaka, S. Suzuki, T. Asaka, K. Yanagida, H. Hanaki, T. Kobayashi, K. Makino, T. Yamane, S. Miyamoto, and K. Horikawa, *Review of Scientific Instruments* **79**, 066102 (2008), https://doi.org/10.1063/1.2940217.
[30] Z. Zhen, Control of Synchrotron X-ray Emission from Laser Wakefield Accelerators, PhD dissertation, University of Michigan (2016).
[31] D. Neely, D. Chambers, C. Danson, P. Norreys, S. Preston, F. Quinn, M. Roper, J. Wark, and M. Zepf, in Superstrong Fields in Plasmas, AIP Conf. Proc. No. 426, edited by M. Lontano, G. Mourou, F. Pegoraro, and E. Sindoni (AIP, New York, 1998) pp. 479{484.
[32] M. Burger, P. J. Skrodzki, J. Lin, J. Nees, K. Krushelnick, and I. Jovanovic, *Opt. Express* **26**, 16456 (2018).
[33] P. Sprangle, C. Tang, and E. Esarey, *IEEE Transactions on Plasma Science* **15**, 145 (1987).
[34] A. J. Goers, G. A. Hine, L. Feder, B. Miao, F. Salehi, J. K.Wahlstrand, and H. M. Milchberg, *Phys. Rev. Lett.* **115**, 194802 (2015).
[35] R. Lehe, M. Kirchen, I. A. Andriyash, B. B. Godfrey, and J.-L. Vay, *Computer Physics Communications* **203**, 66 (2016).

Experiment 2-2019 LaserNetUS: T-CUBED Experiment

Scintillator-based Proton Radiography

PI : Dr. Mario Manuel (General Atomics, 617-899-8381 / manuelm@fusion.gat.com)

Other contributors: Brandon Russell (grad student), Hongmei Tang (grad student), Anatoly Maksimchuk, Louise Willingale (University of Michigan).

Experiments using the T-cubed laser were performed to continue development of a scintillator-based proton radiography system. The goal of these experiments was to demonstrate an understanding of the scintillator response to TNSA protons and to calibrate the imaging system. This technique has been used at facilities in Europe at short-pulse laser facilities, but has not gained traction in the US.

The concept behind the diagnostic is straightforward; incident protons deposit energy into a scintillator which converts this energy into visible light. These photons are collected via standard visible-light optics and transferred to a gated-CCD, either through free-space or via an optical fiber bundle. The back-end CCD may be chosen to accommodate for the extremity of the environment, e.g. radiation-hardened CMOS detectors to handle very high-background systems. In the low-energy experiments designed for T-cubed, our goal was to demonstrate an understanding of the design space and calibrate the front-end for different scintillators. With this understanding, similar diagnostics may be designed specifically for Omega, the NIF, and rep-rated laser facilities.

The demand for proton imaging has dramatically increased in the last 3-5 years due to the growing interest in B-fields in HED plasmas. Moreover, the need for high-rep-rate proton imaging will be of great use to high-power optical laser facilities that are now being combined with high-rep-rate x-ray free electron lasers (XFELs), e.g. at SLAC (United States), SACLA (Japan), or the European XFEL (Germany). The preliminary design for such a system utilizes a filtered scintillator stack coupled to a CCD camera through a fiber optic bundle. Filters are used to block low energy photons and to select a particular proton energy band with which to image. The scintillators are activated as the protons deposit energy in the material and release optical photons that are imaged onto the entrance of an imaging fiberoptic bundle. A gated CCD camera located at the end of the bundle records the image.

During these first experiments using short-pulse-generated protons, radiochromic film (RCF) was used in the filter stack to provide a reference image in a slightly different proton-energy band to be compared with the scintillator-based imaging.

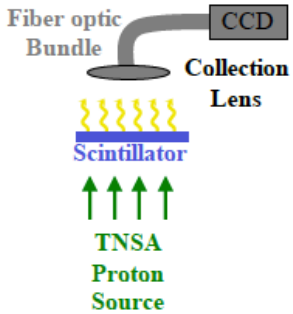

***Fig. 1**: Cartoon schematic of the experimental setup to characterize a scintillator-based proton radiography diagnostic.*

The primary goal of this campaign was to demonstrate a clear understanding of the front-end of this detector, namely the scintillator pack and imaging system. The design to be implemented for these experiments will lay the ground work for future designs that could be implemented at the Omega Facility and the NIF. This technique has only been used with TNSA proton backlighters, and we continued in this regime for these experiments. However, the overall aim was to develop an expertise in this diagnostic technique within the US and to design and build a system that could be used with the popular mono-energetic, D^3He-filled capsule backlighters implemented at Omega and the NIF.

Scintillator-based proton radiography works in a similar fashion as RCF in that both detecting mediums are (in general) sensitive to ions, electrons, and photons. Front filtering is used to protect against signal from low-energy photons, low-energy electrons, and high- Z ions. By using thin scintillators, the diagnostic is sensitive to an energy bandwidth of protons determined by the filtering and subsequent Bragg peak location. Radiation that transmits through the filtering can stimulate emission from the scintillators based on the energy deposition of the radiation. It is therefore imperative to design a filter pack that allows the proton energy of interest to pass, while blocking as much background as possible.

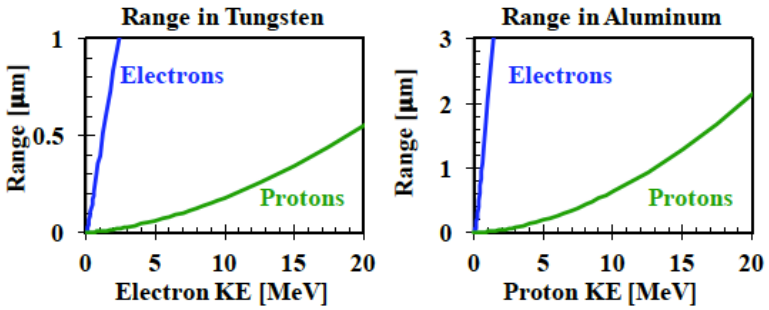

***Figure 2**: Ranges of electrons and protons in tungsten and aluminum.*

For the purposes of these experiments, we focused on a filter-pack designed for <15-MeV protons. Figure 2 illustrates the stopping powers of protons and electrons in tungsten and aluminum. 15-MeV protons have ranges of ~300 μm and ~1.3 mm in tungsten and aluminum, respectively. These same thicknesses will only stop ~800 keV and ~700 keV electrons, respectively, due to the reduced stopping power of electrons relative to protons. In addition to background electrons, we also consider photons created during the laser-matter interaction. From this quick analysis, it is clear that thick, high-Z materials will be preferred to help reduce hard x-ray background, though this does not greatly alter the low-energy-cutoff for relativistic electrons. A solid-state magnet with limited spatial extent can also serve to reduce electron background without altering the proton image since the gyroradius scales nonlinearly with momentum, such that the gyroradius for 1-MeV electrons is ~ 160 times smaller than for a 15-MeV proton; a weak B-field placed well before the scintillator will kick relativistic electrons away while leaving proton trajectories essentially unaltered.

These plastic scintillators are intended for very fast timing applications or when very high pulse pair resolution is required. The use of light guides is best avoided and EJ-228 should be used in small sizes for the best timing results, with the largest scintillator dimensions less than 10 cm to minimize photon scattering effects. This scintillator is particularly useful where very high count rates are present.

PROPERTIES	EJ-228	EJ-230
Light Output (% Anthracene)	67	64
Scintillation Efficiency (photons/1 MeV e⁻)	10,200	9,700
Wavelength of Maximum Emission (nm)	391	391
Light Attenuation Length (cm)	-	120
Rise Time (ns)	0.5	0.5
Decay Time (ns)	1.4	1.5
Pulse Width, FWHM (ns)	1.2	1.3
H Atoms per cm³ (×10²²)	5.15	5.15
C Atoms per cm³ (×10²²)	4.69	4.69
Electrons per cm³ (×10²³)	3.33	3.33
Density (g/cm³)	1.023	1.023

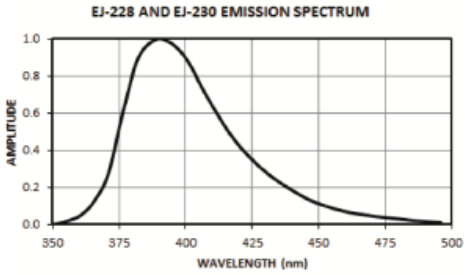

Figure 3: *Specifiucation sheet*

Reducing the incident background (electrons and photons) using filters was the first step in producing a high-quality proton image, the next is using thin scintillators. For these experiments, we tested multiple scintillator types from Eljen Technologies: EJ-228, EJ- 204, EJ-212. Each emits in a slightly different optical bandwidth with varying decay times.

EJ-212 was chosen for comparison with previous work [1]. However, EJ-228 was the main focus of these experiments (see Figure 3) due to its superior decay time (~ .4 ns). We ordered 3 thicknesses of EJ-228 to test: 50μm, 100μm, and 500 μm. Thinner scintillators produce higher energy resolution (sensitive to a thinner bandwidth) and reduced background at the cost of lower signal levels (optical emission caused by proton stopping). Optical images are created by collecting emission from the entire scintillator using a lens to generate an image onto a fiber optic bundle coupled to a gated-CCD. The campaign at T-cubed provided the means to quantify design trade-offs experimentally and verify modeling of this diagnostic for future designs to be used at other facilities.

The T-cubed laser was used with maximum energy at peak compression. Recent work on T-cubed demonstrated proton imaging using RCF with reasonable proton with energies of up to 10-MeV which was suffcient to experimentally test the scintillator response to protons with a real background from a laser-generated source.

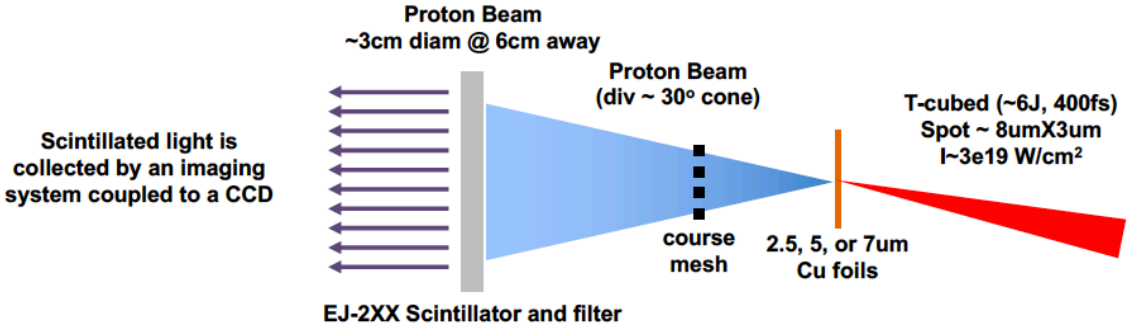

Figure 3*. Experimental setup*

The steps in the experiemntal run were as follows:
Optimize proton source for high energy and reliability (2.5, 5, or 7um copper) using TP
• Measure imaging resolution with large grid on the back of the scintillator
• Filter steps were then used, e.g. 10um and 50um Al, that will have minimal effect on electrons, but a dramatic effect on protons

As a result of these experiments in March 2019 a significant amount of data on the performance of these scintillators was obtained. The data is presently being anayzed.

References

[1] J. S. Green, M. Borghesi, C. M. Brenner, D. C. Carroll, N. P. Dover, P. S. Foster, P. Gallegos, S. Green, D. Kirby, K. J. Kirkby, P. McKenna, M. J. Merchant, Z. Najmudin, C. A. J. Palmer, D. Parker, R. Prasad, K. E. Quinn, P. P.Rajeev, M. P. Read, L. Romagnani, J. Schreiber, M. J. V. Streeter, O. Tresca, C. G. Wahlstrom, M. Zepf, and D. Neely. “Scintillator-based ion beam pro_ler for diagnosing laser-accelerated ion beams". Proceedings of SPIE, 8079, 807919 (2011).

[2] N. Cook, O. Tresca, and R. Lefferts, “Scintillator diagnostics for the detection of laser accelerated ion beams". *Journal of Instrumentation*, 9(09), P09004 (2014).

[3] Manuel, M. J.-E., C. C. Kuranz, A. M. Rasmus, S. Klein, M. J. MacDonald, M. R. Trantham, J. R. Fein, P. X. Belancourt, R. P. Young, P. A. Keiter, R. P. Drake, B. B. Pollock, J. Park, A. U. Hazi, G. J. Williams, and H. Chen. “Experimental results from magnetized-jet experiments executed at the Jupiter Laser Facility", *High Energy Density Physics*, 17, 52 (2014).

[4] S. R. Klein, Manuel, M. J.-E., B. B. Pollock, R. S. Gillespie, M. Deininger, C. C. Kuranz, P. A. Keiter, and R. P. Drake, “Construction of a solenoid used on a magnetized plasma experiment". *Review of Scientific Instruments*, 85(11), 11E812 (2014).

Experiment 3-2020 LaserNetUS: Hercules experiment (Shahani)

High resolution Microtomography of Quasicrystalline Alloys using a Laser-Driven X-ray Betatron Source

PI : Professor Ashwin Shahani: Dept. of Material Science and Engineering, University of Michigan, Ann Arbor

This experiment is ongoing and initial data collection is underway as of November 2020.
The following is a recap of the ongoing experiment from the proposal.

Laser wakefield acceleration [1, 2, 3] is a method for generating high energy electron beams by coupling ultrashort pulsed lasers to extremely hot matter, i.e. the fourth state of matter, plasma. In laser wakefield acceleration, an electron bunch “surfs" on the electric wave generated by the light pressure of an intense laser [4]. This plasma wave has a strong longitudinal electric field that stays in phase with the relativistic driver. Therefore, a relativistic charged particle can also remain in phase with the accelerating field over long distances and gain significant energy. The accelerating electric field strength that the plasma wave can support can be many orders of magnitude higher than that of a conventional accelerator. The astonishing field strengths are equivalent to the 2 mile long accelerator used for the Laser Coherent Light Source at Stanford being reduced to less than half a meter in length. The wakefield also has strong transverse fields that oscillate the electrons, causing them to radiate X-rays. These X-rays are of ultrashort temporal duration, small source size for high resolution and are spatially coherent.

The X-ray source will then be used to obtain transmission images of sub-mm scale complex microstructures (e.g., quasicrystals) at multiple projection angles. Quasicrystals (QCs), or “nature’s forbidden crystals" as they are sometimes called, have stimulated considerable research activity since their discovery in 1984 (see Fig. 1). They are defined as crystal structures that are ordered but aperiodic. However, QCs are much more than crystallographic curiosities: interestingly, they feature high electrical and thermal resistivity, unexpected for a material containing aluminum (Al) as the major constituent. For this reason, it is anticipated that QCs may be incorporated in heat insulating layers and temperature sensors. Still, several fundamental questions need to be answered prior to commercialization. For instance, what are the equilibrium and kinetic shapes of the QCs?

Are they entropically or energetically stabilized? These questions can only be addressed by measuring in three dimensions (3D) the QC-containing and Al-based microstructures grown under various solidification pathways. The resultant microstructures are often complex in the sense that they consist of not only QC phases but also periodic intermetallic (approximant) phases as well as multi-phase eutectics. Through X-ray tomographic imaging of our alloy samples, we can establish for the first time the thermophysical regimes of QC stability and morphology.

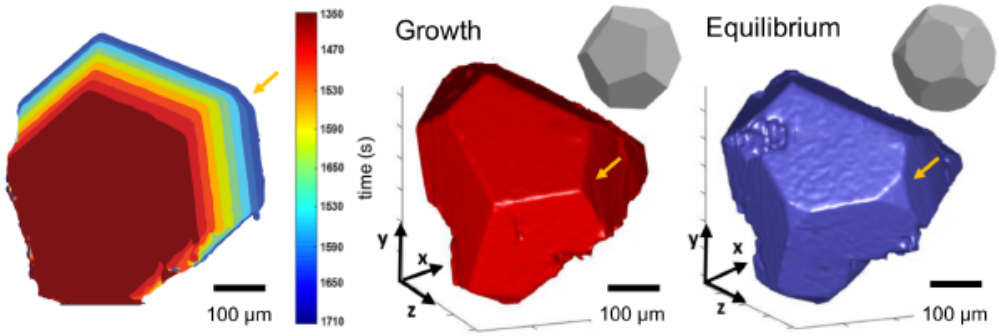

Figure 1: *[N. Senabulya, I. Han, X. Xiao, A.J. Shahani, Scripta Mater. 146, 218 (2018)] (left) Two-dimensional isochrones of a solid Al-Pd-Mn icosahedral during solidification, where color indicates the passage of time. 3D renderings of the QC at an early stage of growth (middle) and at a later stage (right). Note the change in structure between the two stages (inset).*

The specific aims of the experiment are:
-Produce stable and energy tunable electron beams at 5 Hz repetition rate.
-Optimize the electron beams for X-ray production at 5 keV critical energy.
-Perform tomography of the quasicrystal sample.

Experimental Procedure

The experimental procedure will be as follows:
1. Produce the pump electron beam. Fully characterize the electron beam parameters, i.e, electron beam energy, total charge, source size, divergence angle, pointing stability. This should be completed within 1 week. We plan to use 3D printed gas cells with variable gas length. Therefore we will measure the plasma density as a function of backing pressure with transverse interferometry. This will require a low energy laser pulse as the probe.

2. Measure the X-ray production over a wide range of parameters. Establish best parameters for source size.

Technical Feasibility

T he X-ray betatron source and imaging capabilities has been demonstrated on Hercules already. The high rep rate operation will allow rapid tomography of the quasicrystal structure. To quantify the compositional changes we have developed a multilayer scintillator detector. This idea was first introduced in Ref. [5], albeit for synchrotron-based X-ray imaging. The scheme relies on two scintillator materials that are doped differently (e.g., commercially available LSO:Tb and LYSO:Ce) so as to emit a different wavelength of optical light. A dichroic mirror separates the emission spectra into two optical channels which are directed onto two high resolution CCD systems. In this way, we can record a low- and high-energy X-ray projection image simultaneously with micrometer spatial resolution. From the collected spectral information, we can then discriminate between different material compositions, which would otherwise not be possible with a single projection image and/or without sacrificing temporal resolution in the in situ experiment.

The broad-band laser-wakefield accelerator generated X-ray source can be used for phase-contrast imaging in a projection-based geometry. For small refractive index gradients, the phase contrast pattern is essentially a ray tracing effect, with X-rays being directed into dark and light regions by deection in the refractive index gradients [6]. For a polychromatic source, phase contrast is still possible as the intensity pattern generated is independent of wavelength to first

order in the paraxial approximation.

Plasma accelerator X-ray source phase-contrast imaging studies typically use propagation based phase-contrast imaging, with a spherical wave expanding from a micron-scale source leading to spatial coherence after a short propagation distance l to an object plane. A phase-image forms some distance L after the object due to interference between the rays that are deected by refractive index gradients. If the gradients are strong, the paraxial approximation breaks down and a Fresnel-Kirchoff approach must be used instead [7]. The X-ray beam must therefore have spatial coherence, i.e. a phase correlation across the wave front, over a length larger than the scale-length associated with the gradients.

Since we expect to resolve features at the image plane, therefore the transverse coherence length should be longer than the source size, and we can calculate the source-object distance. For example, for 10 keV X-rays with a 3 μm source size, the coherence length is at least the source size when the source to object distance is 45 cm.

Equipment

Gas target system. The gas system including the gas target for electron beam generation is required. For the electron generation, we will to use the 3D printed, 2 stage gas target system developed at Hercules.

Diagnostics. We will use standard LWFA experiment diagnostics for electron beam profile and spectra, including electron spectrometer, scintillating screens, CCDs. The scintillating screens should be able to be installed both before and after the electron spectrometer so we can measure the filaments before and after the electron spectrometer. 2-color X-ray imaging will be provided by scintillators/CCD cameras developed by the Shahani group.

Targets. We will use quasicrystal samples grown by the Shahani group.

Parameters

The experiment will last 3 weeks access to the Hercules 5 Hz laser. We require the standard laser parameters for generating relativistic electron beams. pulse length 35 fs, peak power P > 50 TW, f/20 focusing optic.

_ Week 1: Electron optimization
_ Week 2: X-ray optimization
_ Week 3: Tomography of sample.

The basic experimental setup is illustrated in Fig.2.

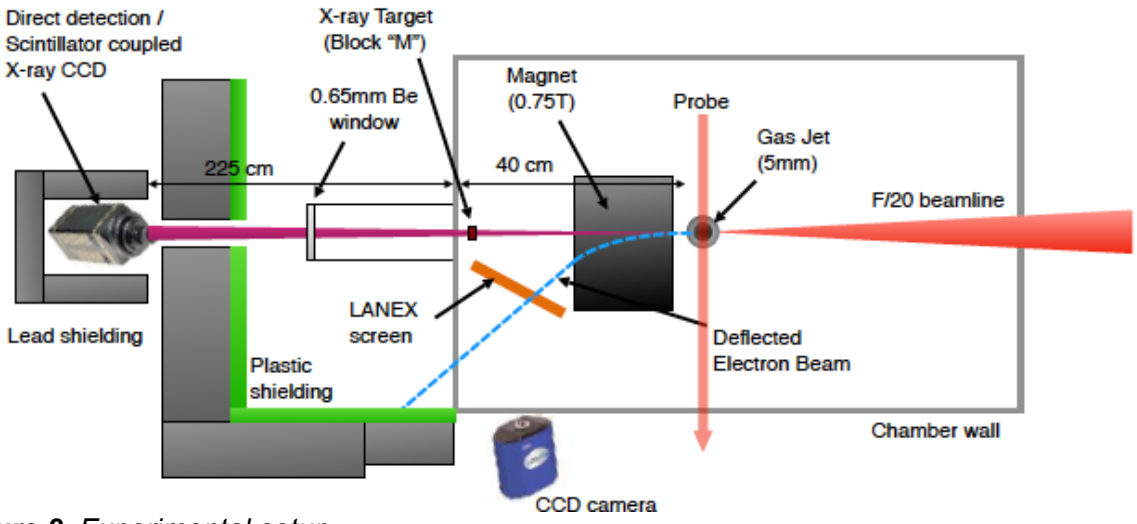

Figure 2. *Experimental setup.*

References

[1] S. P. D. Mangles, et al., *Nature*, **431**, 535 (2004).
[2] C. G. R. Geddes, et al., *Nature*, **431**, 538 (2004).
[3] J. Faure, et al., *Nature*, **431**, 541 (2004).
[4] T. Tajima and J. M. Dawson, *Phys. Rev. Lett.*, **43**, 267 (1979).
[5] D. Modgil, et al., *Phys. Med. Biol.*, **60**, 8025 (2015).
[6] S. Wilkins, et al., *Nature,* **384**, 335 (1996).
[7] A. Pogany, D. Gao, and S. W. Wilkins, *Rev. Sci. Instr.*, **68**, 2774 (1997).
[8] S. Kneip, et al., *Nature Physics*, **6**, 980 (2010).
[9] J. Cole, et al., *Scientific Reports*, **5** (2015).